J MATER SCI 41 (2006) 4169–4177

Effect of thermal conductivity on reaction front propagation during combustion synthesis of intermetalics

M. BALLAS, H. SONG, O. J. ILEGBUSI*
Department of Mechanical, Materials and Aerospace Engineering, University of Central Florida, Orlando, FL 32816-2450
E-mail: ilegbusi@mail.ucf.edu

Published online: 15 May 2006

A mathematical model is developed to investigate the effect of thermal conductivity on the combustion synthesis of intermetallics. The governing equations are solved using a high-order-implicit numerical scheme capable of accommodating the steep spatial and temporal gradients of properties. A parametric study is then performed to elucidate reaction characteristics (propagation type, steady-state propagation velocity, peak temperature, etc.) in terms of the thermal conductivity ratio, $\kappa = k_p/k_r$. The predicted results appear plausible and consistent with the trends presented in the available literature.

1. Introduction

The production of certain ceramics, intermetallics, and composite materials by self-propagating high-temperature synthesis (SHS) has become increasingly popular due to its many advantages over conventional production techniques. These benefits include low cost/energy requirements, high homogeneity throughout the product, reduced microstructural segregation, low contamination, and the relative simplicity of the process [1, 2]. The growing popularity of SHS has led to a number of experimental, theoretical and numerical studies aimed at improving our understanding of the processes involved [1–4]. However, existing theoretical and numerical studies have typically relied on oversimplifications such as the assumption of constant thermal conductivity throughout the specimen. Further work is therefore desirable to elucidate the effects of variable thermophysical properties. This is the subject of the present paper.

By definition, SHS involves initiating an exothermic, condensed-phase chemical reaction between two or more species to obtain the desired product. There exist two distinct modes of SHS, differing primarily in the manner in which the reaction progresses. The first, commonly referred to as combustion synthesis, involves igniting the constituent powder compact at one or more surfaces and allowing the reaction front to propagate as a combustion wave throughout the remaining material. In the second mode (i.e. explosion synthesis), the temperature of the powder compact is raised above the ignition point of the system thus allowing the entire mass to react simultaneously.

While under the appropriate conditions the exothermic nature of the reaction allows the process to become steadily self-sustaining, SHS is very sensitive to the process parameters and material properties and other reaction patterns are possible (i.e. oscillatory propagation, fingering, and reaction extinction) [5–7].

In order to fully realize the potential of SHS, it is imperative that the individual and cumulative effects of the various material and process parameters on the characteristics of both the reaction itself and the final product be fully understood. Process parameters such as preheat temperature, porosity, and the amount of reactant dilution, have all been shown experimentally to have a strong effect on the behavior of the combustion synthesis process [6, 8–13]. The material properties of the various phases also influence the reaction significantly [4, 6, 13, 14]. Thus, there have been numerous attempts to model SHS to study the process through numerical experiments, and to apply existing knowledge for optimization of industrial SHS processes.

Experimental data and numerical analysis both suggest that the effective thermal conductivity, k_{eff}, is one of the most important parameters impacting reaction behavior

*Author to whom all correspondence should be addressed.
0022-2461
DOI: 10.1007/s10853-006-6751-0

during combustion synthesis [5, 10, 15, 16]. This influence is further complicated by temporal and spatial variations in k_{eff} arising from its functional dependence on a number of parameters, both material and otherwise. These parameters include species concentration, temperature, and porosity. While a number of previous studies of combustion synthesis have included different conductivities for the different phases [16, 17], very little has been done to specifically explore the effects of variable thermal conductivity on the reaction characteristics. This issue is particularly important when considering the effect of non-material (morphological) parameters such as porosity, particle size, particle packing, etc., as these are all expected to significantly affect the propagation of the reaction front during synthesis. For example, a number of authors have reported an increase in porosity behind the reaction front, possibly due to the rapid expansion of trapped gas within the interstitial pores [3, 18]. This increase in porosity undoubtedly affects k_{eff}, potentially leading to a large conductivity gradient ($\partial k_{\text{eff}}/\partial z$) in the vicinity of the reaction front.

In this paper, the effect of thermal conductivity on the behavior of the combustion synthesis process is investigated. Specifically, differences in the effective thermal conductivity on either side of the reaction front accompanied by a conductivity gradient in the reaction zone itself are considered. Fig. 1 illustrates the combustion synthesis process and the associated differences in effective thermal conductivity for the reactant, combustion and product phases. While in practice these differences may be either material or process dependent, the exact source is of less concern than the overall effect on the propagation of the reaction front. A model is developed to simulate the process taking into account variations in k_{eff} as the reaction progresses. A parametric study is then performed to elucidate reaction characteristics (propagation type, steady-state propagation velocity, peak temperature, etc.) in terms of the thermal conductivity ratio, $\kappa = k_p/k_r$.

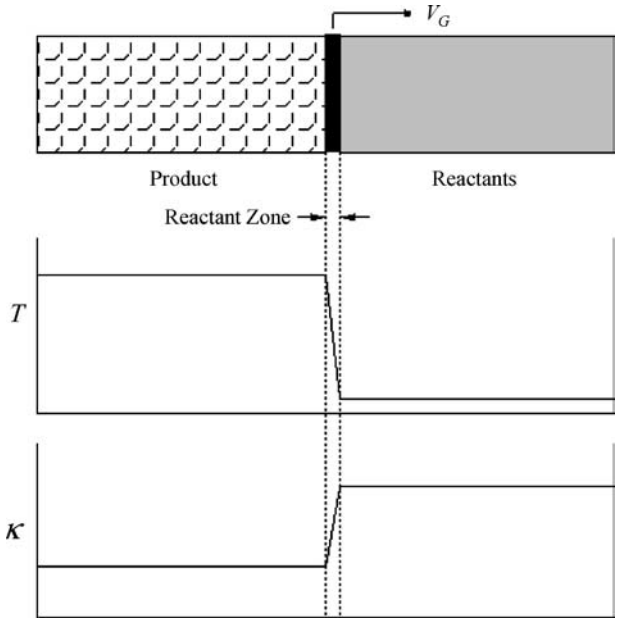

Figure 1 Schematic of the combustion synthesis process, the corresponding temperature profile, and the effective thermal conductivity for the reactant, combustion, and product regions.

2. Formulation

2.1. Governing equations

Simulation of solid-solid combustion synthesis requires the simultaneous solution of the coupled equations for energy conservation and chemical reaction. Assuming negligible mass transfer (i.e. limited liquid phase convection through the powder compact), the adiabatic energy equation can be expressed as a simple, one-dimensional transient heat conduction equation:

$$\rho c_p \frac{\partial T}{\partial t} = \frac{\partial}{\partial z}\left(k_{\text{eff}} \frac{\partial T}{\partial z}\right) + \dot{S} \tag{1}$$

where ρ is the density, c_p is the specific heat, T is the temperature, k_{eff} is the effective thermal conductivity of the bulk material, z and t are the spatial and temporal coordinates, respectively, and $\dot{S}$ is a source term accounting for the energy produced by the reaction.

Assuming a stoichiometric mixture of reactant powders, the Arrhenius type nth-order rate equation describing the reaction kinetics takes the following form:

$$\dot{S} = \rho \Delta H_f \cdot \exp\left(-\frac{Q_R}{R_G T}\right)\left(1 - f_p\right)^n \tag{2}$$

where ΔH_f is the heat of reaction, A is the frequency factor, Q_R is the activation energy, R_G is the gas constant, f_p is the fraction of the product phase, and n is the order of the reaction.

For the specific case considered here in which $k_{\text{eff}} = k_{\text{eff}}(z)$, Equation 1 can be expanded as follows:

$$\rho c_p \frac{\partial T}{\partial t} = k_{\text{eff}} \frac{\partial^2 T}{\partial z^2} + \frac{\partial k_{\text{eff}}}{\partial z}\frac{\partial T}{\partial z} \tag{3}$$

Note that in cases where k_{eff} in the reaction and product zones differ significantly, the second term on the right hand side of Equation 3 is expected to figure prominently near the reaction zone due to the large conductivity gradients.

2.2. Non-dimensionalization

The governing equations can be non-dimensionalized by defining the following relations:

$$\overline{T} = \frac{T}{T^*}, \quad \overline{H} = \frac{H}{c_p T^*}, \quad \overline{t} = \frac{t}{t^*}$$
$$\overline{z} = \frac{z}{z^*}, \quad \overline{k} = \frac{k_{\text{eff}}}{k^*}, \quad \gamma = \frac{Q_R}{R_G T^*} \tag{4}$$

where T^* and k^* are reference values for temperature and thermal conductivity, respectively, and the remaining starred terms are defined as:

$$t^* = \frac{\exp(\gamma)}{A}, \quad z^* = \left(\frac{k^* t^*}{\rho c_p}\right)^{1/2} \tag{5}$$

Within this framework, Eq. 3 can be expressed in non-dimensional form as:

$$\frac{\partial \overline{T}}{\partial \overline{t}} = \overline{k}\frac{\partial^2 \overline{T}}{\partial \overline{z}^2} + \frac{\partial \overline{k}}{\partial \overline{z}}\frac{\partial \overline{T}}{\partial \overline{z}} + \overline{\dot{S}} \tag{6}$$

Similarly, Eq. 2 becomes:

$$\overline{\dot{S}} = \Delta H_f \cdot \exp(\gamma(1 - 1/\overline{T}))(1 - f_p)^n \tag{7}$$

A non-adiabatic form of Eq. 6 that takes into account convection and radiation at the exposed surface is:

$$\frac{\partial \overline{T}}{\partial \overline{t}} = \overline{k}\frac{\partial^2 \overline{T}}{\partial \overline{z}^2} + \frac{\partial \overline{k}}{\partial \overline{z}}\frac{\partial \overline{T}}{\partial \overline{z}} + C_1(\overline{T}_\infty - \overline{T}) + C_2(\overline{T}_\infty^4 - \overline{T}^4) + \overline{\dot{S}} \tag{8}$$

where $\overline{T}_\infty$ is the dimensionless ambient temperature and C_1 and C_2 are the dimensionless heat transfer coefficients for convection and radiation, respectively. The coefficients are defined as:

$$C_1 = \frac{2h}{R_N}\left(\frac{t^*}{\rho c_p}\right), \quad C_2 = \frac{2\sigma\varepsilon}{R_N}(T^*)^3\left(\frac{t^*}{\rho c_p}\right) \tag{9}$$

where R_N is the radius of the cylindrical cross-section.

3. Numerical solution procedure

3.1. Operator compact implicit method

Due to the steep spatial and temporal gradients inherent in combustion synthesis, a high-order compact finite difference scheme is adopted to approximate the governing equations. This approach provides an improved representation of the different length scales over the standard central differencing scheme, thereby increasing spatial accuracy to a nearly spectral-like resolution [19]. While a standard high-order scheme is appropriate in cases where k_{eff} is assumed constant [7, 14], the mixed order derivatives apparent in Equations 6 and 8 require an alternative approach [20, 21].

The operator compact implicit (OCI) method allows accurate representation of mixed derivatives of the type [20]:

$$L(u) = a(x)u_{xx} + b(x)u_x = f \tag{10}$$

Rather than approximating the individual derivatives, the OCI method involves obtaining a relationship between the spatial derivative operator, $L(u)$, and the function u. Furthermore, by limiting the stencil size to three adjacent points, the tridiagonality of the matrices is retained, thus solutions are readily obtainable. The tridiagonal OCI relationship takes the form:

$$q_i^+(L(u))_{i+1} + q_i^o(L(u))_i + q_i^-(L(u))_{i-1} = \frac{r_i^+ u_{i+1} + r_i^o u_i + r_i^- u_{i-1}}{h^2} \tag{11}$$

where h is the node width and the q_i and r_i terms are both functions of the spatial derivative coefficients as defined in [20]:

$$q_i^+ = 6a_i a_{i-1} + h(5a_{i-1}b_i - 2a_i b_{i-1}) - h^2 b_i b_{i-1} \tag{12}$$

$$q_i^o = 4[15a_{i+1}a_{i-1} - 4h(a_{i+1}b_{i-1} - a_{i-1}b_{i+1}) - h^2 b_{i+1}b_{i-1}] \tag{13}$$

$$q_i^- = 6a_i a_{i+1} - h(5a_{i+1}b_i - 2a_i b_{i+1}) - h^2 b_i b_{i+1} \tag{14}$$

$$r_i^+ = \frac{1}{2}\left[q_i^+(2a_{i+1} + 3hb_{i+1}) + q_i^o(2a_i + hb_i) + q_i^-(2a_{i-1} - hb_{i-1})\right] \tag{15}$$

$$r_i^- = \frac{1}{2}\left[q_i^+(2a_{i+1} + hb_{i+1}) + q_i^o(2a_i - hb_i) + q_i^-(2a_{i-1} - 3hb_{i-1})\right] \tag{16}$$

$$r_i^o = -(r_i^+ + r_i^-) \tag{17}$$

For the case of adiabatic combustion synthesis with variable thermal conductivity, $\overline{k}$:

$$L(\overline{T})_i = \left\{\frac{\partial \overline{T}}{\partial \overline{t}} - \overline{\dot{S}}\right\}_i \tag{18}$$

and

$$q_i = q(a_i, b_i) = q\left(\overline{k}, \frac{\partial \overline{k}}{\partial \overline{z}}\right)_i, \quad r_i = r(a_i, b_i) = r\left(\overline{k}, \frac{\partial \overline{k}}{\partial \overline{z}}\right)_i \tag{19}$$

Relationships for the non-adiabatic case can be similarly obtained by adding the C_1 and C_2 terms of Eq. 8 to $L(\overline{T})$.

3.2. Computational details

The algebraic equations are integrated over spatial and temporal grids that have been systematically optimized to obtain sufficient numerical accuracy of the solution.

TABLE I. Material properties used in the computations

Parameter	Units	NiTi	Mg_2Ni
ρ	kg/m^3	6450	2860
c_p	J/kg·K	439.0	483.8
ΔH_f	kJ/mol	−66.5	−372.4
A	s^{-1}	3.0×10^9	5.46×10^8
Q_R	kJ/mol	201	159
N		2	2

This process results in the choice of time steps in the range 6.25×10^{-9} to 5.0×10^{-6} s and node spacings of 1.0×10^{-7} to 1.0×10^{-5} m, depending on the complexity of the specific reaction.

Two representative material systems were considered in this study: NiTi and Mg_2Ni. The relevant thermophysical properties for the reactions are provided in Table I.

4. Results and discussions

Fig. 2a shows the dimensionless temperature $\overline{T}_0$ profiles at consecutive times for the adiabatic combustion synthesis of NiTi with conductivity ratio $\kappa = k_p/k_r = 5.0$. The corresponding product fraction profiles are shown in Fig. 2b. For this value of κ, the reaction assumes a steady propagation profile following the initial preheat and ignition stages. For the NiTi reaction initiated in compacts preheated to $\overline{T}_0 = 0.51$ ($T_0 = 600$ K), this steady profile appears to be representative of all $\kappa > 1.0$.

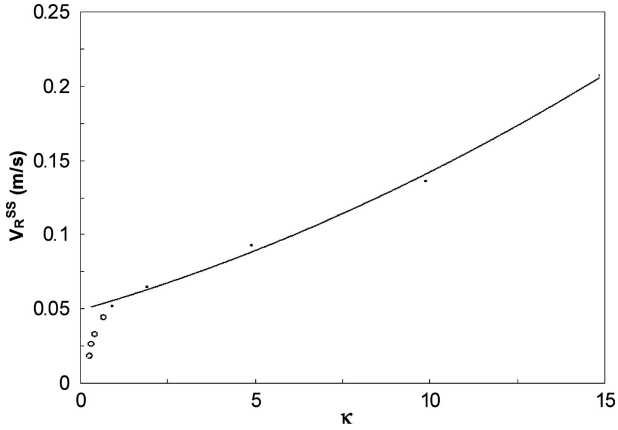

Figure 3 Steady-state reaction velocity, v_R^{ss}, versus κ for combustion synthesis of NiTi.

Fig. 3 depicts the steady state reaction front velocity, v_R^{ss}, as a function of κ for the NiTi system. The velocity was calculated from the data using the following equation:

$$v_R^{ss} = \frac{(z_B - z_A)\Delta z}{(t_B - t_A)\Delta t} \tag{20}$$

where z_A and z_B are nodes at the ends of the region of steady state propagation and t_A and t_B are the corresponding time steps at which the reaction front reaches

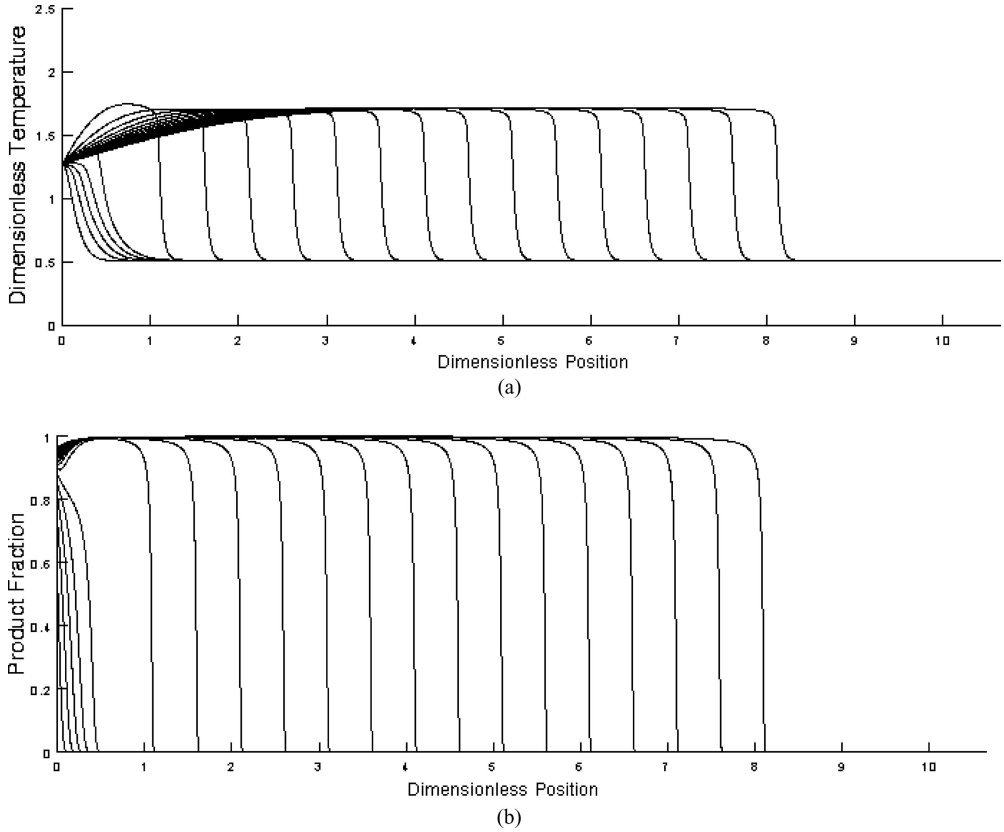

Figure 2 Plot of (a) dimensionless temperature, $\overline{T}$, and (b) product fraction, f_p, profiles: NiTi, $\kappa = 5.0$, $\Delta t = 5.0 \times 10^{-3}$ s.

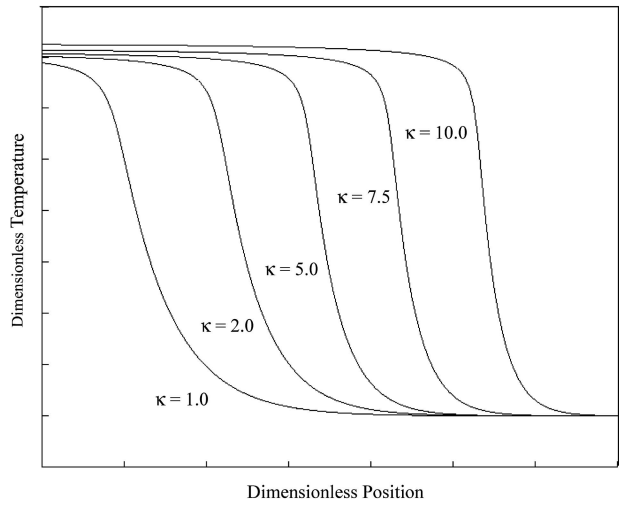

Figure 4 Representative temperature profiles at the reaction front during NiTi synthesis for various values of κ.

nodes A and B, respectively. The data predicts an exponential increase in v_R^{ss} with increasing κ. This trend appears somewhat counterintuitive since a higher thermal conductivity ahead of the reaction front might be expected to help to preheat and ignite the reactants. Rather, the opposite behavior is observed. This trend is probably attributable to the development of a thinner reaction zone with increasing κ. In other words, a lower conductivity ahead of the reaction front helps to concentrate the heat generated during the reaction in the adjacent, unreacted 'layer'. Thus, most of the available energy is used to ignite the adjacent reactants rather than allowing the energy to diffuse too far ahead of the reaction zone. This behavior is illustrated in Fig. 4, which shows the temperature profile in the vicinity of the reaction zone for various values of κ. An increase in κ (corresponding to a decrease in k_r, assuming constant k_p) results in a steeper temperature gradient and thus a thinner reaction zone.

While the reaction propagates steadily for $\kappa > 1.0$, at $\kappa = 1.0$ the steady propagation front ultimately degenerates into an oscillatory pattern as shown in Fig. 5. For $\kappa < 1.0$, the oscillatory propagation front develops immediately as illustrated in Fig. 6 for the case of $\kappa = 0.5$. These observations can again be explained in terms of the thickness of the reaction front. While the reaction zone remains relatively thin in the case of steady propagation, the temperature gradient decreases significantly as a result of the high thermal conductivity ahead of the reaction below $\kappa = 1.0$. The reduced temperature gradient coupled with a slower propagation velocity causes extensive preheating well ahead of the reaction front without the immediate onset of combustion. Ultimately, this preheating results in the bulk ignition of a portion (i.e., multiple layers) of

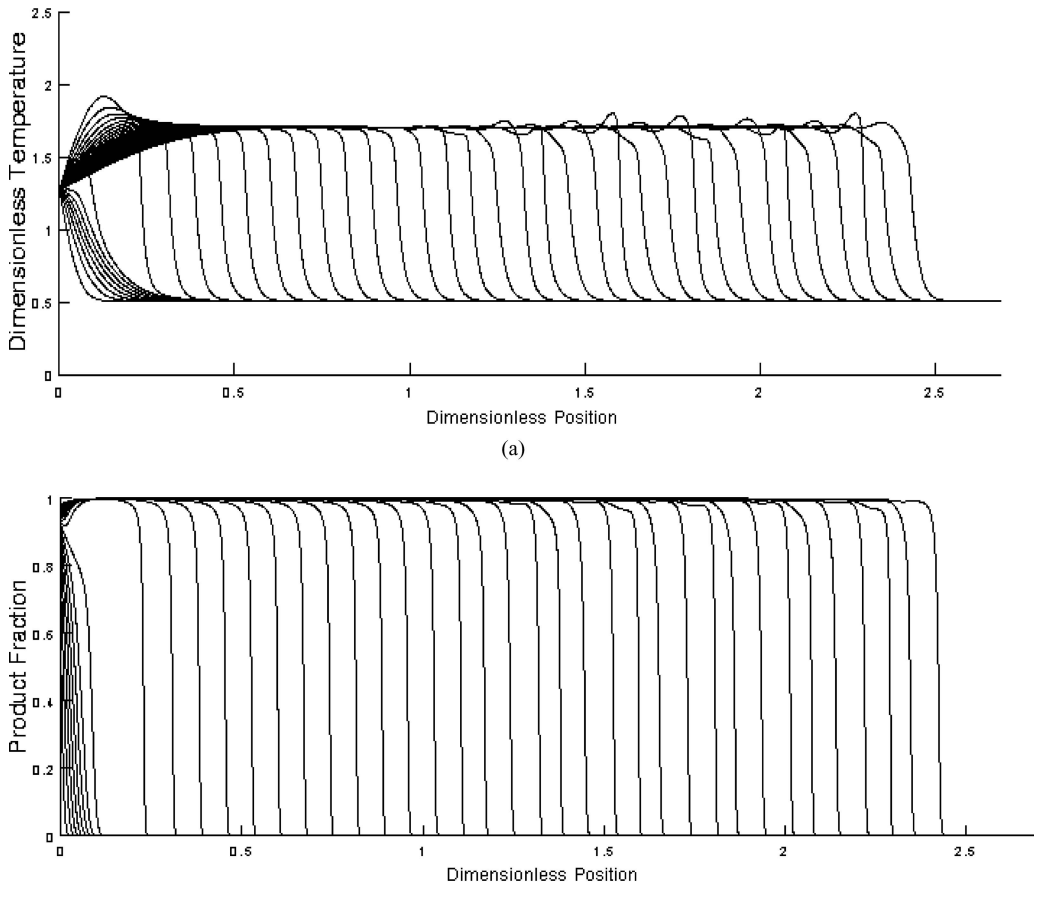

Figure 5 Plot of (a) dimensionless temperature, $\overline{T}$, and (b) product fraction, f_p, profiles: NiTi, $\kappa = 1.0$, $\Delta t = 5.0 \times 10^{-3}$ s.

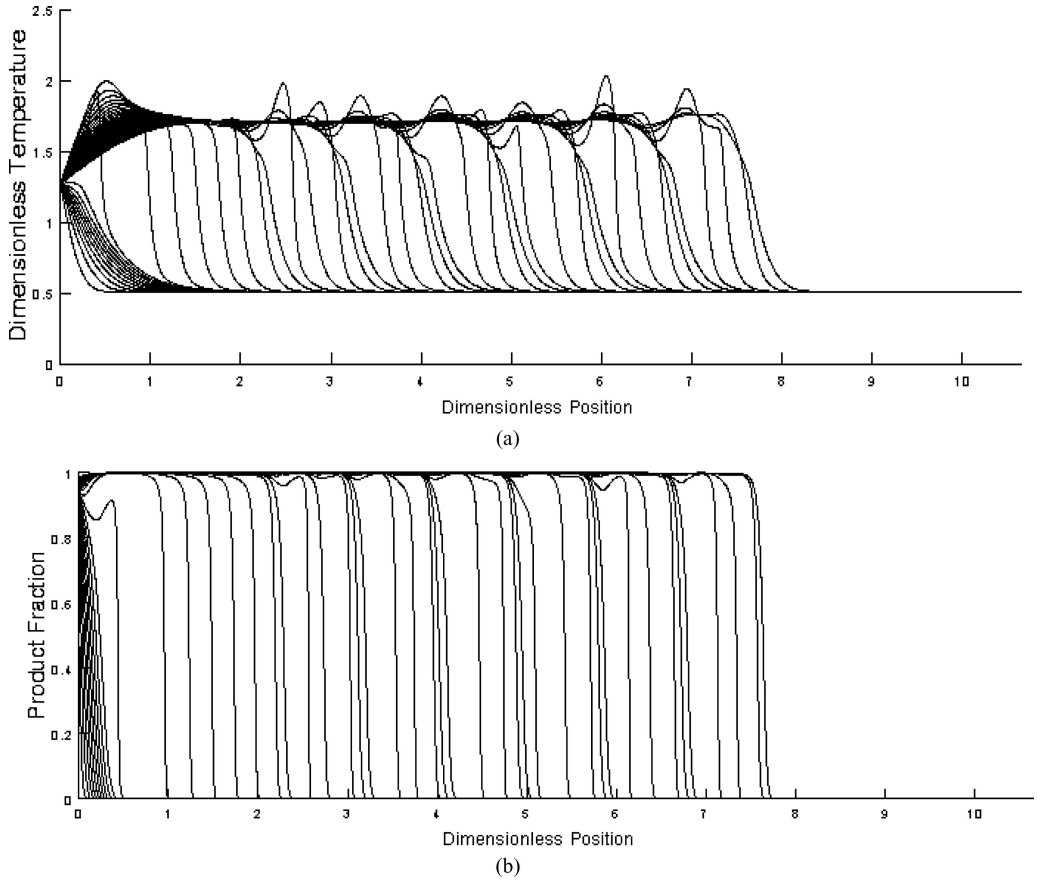

Figure 6 Plot of (a) dimensionless temperature, $\overline{T}$, and (b) product fraction, f_p, profiles: NiTi, $\kappa = 0.5$, $\Delta t = 5.0 \times 10^{-3}$ s.

the reactants. Heat is then conducted ahead of the bulk reaction zone and the process repeats itself, leading to the observed oscillatory pattern.

When the average propagation velocity data for the oscillatory cases are included in the Figure (represented by 'o' in Fig. 3) with the steady propagation data, a sharp deviation from the established trend is observed. Rather than maintain a linear dependence on κ, the average propagation velocity decreases much more quickly with decreasing κ. Furthermore, no self-sustaining synthesis was observed for $\kappa = 0.1$, even after a prolonged ignition period. This result indicates that explosion (bulk) synthesis is the only feasible synthesis mode in systems exhibiting a κ value below a certain threshold.

For comparative purposes, additional cases were simulated using thermophysical properties approximating those of the Mg_2Ni system (see Table I). In terms of their effect on reaction behavior, the most significant differences between the two systems are the higher enthalpy of formation (ΔH_f), lower activation energy (Q_R), and lower density (ρ) associated with Mg_2Ni.

Fig. 7(a) shows the dimensionless temperature profiles at consecutive times for the adiabatic combustion synthesis of Mg_2Ni for $\kappa = 5.0$ and $\overline{T}_0^{Mg_2Ni} = \overline{T}_0^{NiTi} = 0.51$. The corresponding product fraction profiles are shown in Fig. 7(b). As was the case for NiTi ($\kappa = 5.0$), the reaction assumes a steady propagation profile following the initial preheat and ignition stages. However, unlike the NiTi system which develops propagation instabilities below $\kappa = 1.0$, the Mg_2Ni system exhibits no such instabilities throughout the entire range of interest ($0.1 < \kappa < 15.0$).

Fig. 8 shows the steady state reaction front velocity, v_R^{ss}, as a function of κ for the Mg_2Ni system. As expected, the data predicts an increase in v_R^{ss} with increasing κ though the relationship is not quite as pronounced as that observed in the NiTi system. A two order-of-magnitude increase in κ results in about 117% increase in v_R^{ss} while an increase of almost 160% was observed in the case of NiTi for a single order-of-magnitude increase in κ. Thus, for the range of κ values investigated here, v_R^{ss} appears to be approaching a maximum propagation velocity. This result seems to agree with the limiting expression developed for the reaction propagation velocity assuming an infinitely thin reaction zone [12, 15, 22].

The differences between the behaviors of the two systems at low κ are likely due to the high adiabatic reaction temperature, T_a, associated with Mg_2Ni synthesis ($T_a \equiv \Delta H_f / \rho c_p = 7174$ K versus 1422 K for NiTi). A higher reaction temperature tends to promote ignition in the adjacent reactant layer before a significant amount of heat can diffuse ahead of the reaction zone, even in cases where the thermal conductivity ahead of the reaction is significantly larger than that in the product region (i.e. low values of κ). Thus, the reaction propagation velocity, v_R,

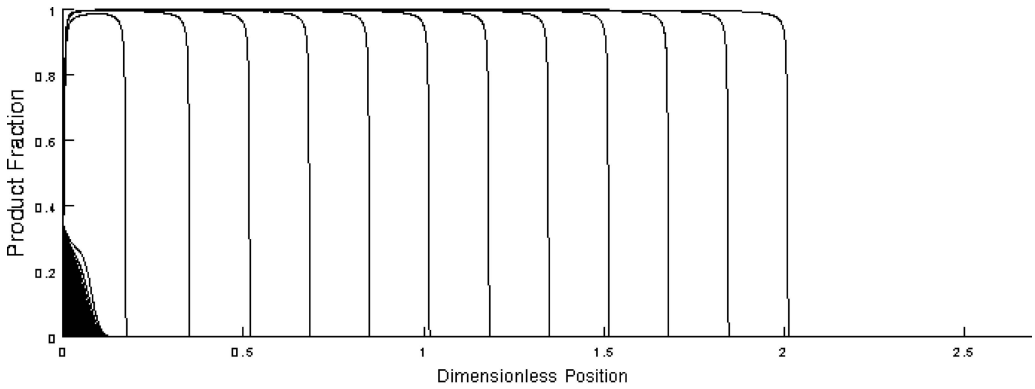

(a)

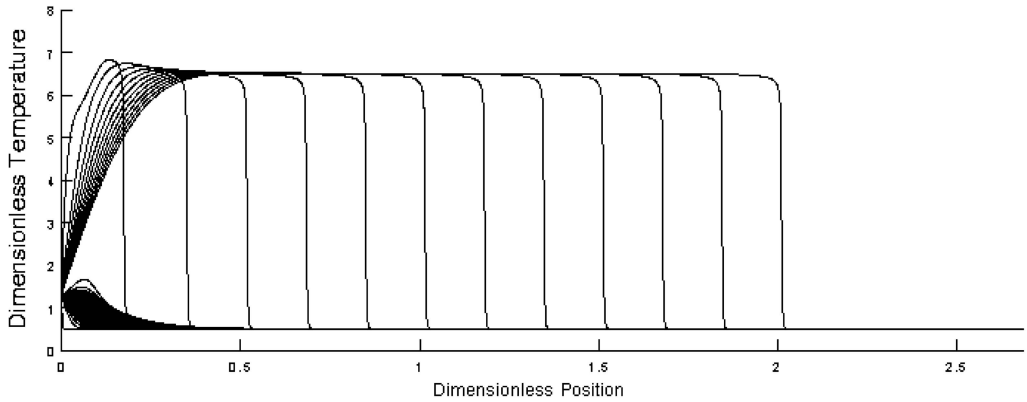

(b)

Figure 7 Plot of (a) dimensionless temperature, $\overline{T}$, and (b) product fraction, f_p, profiles: Mg_2Ni, $\kappa = 5.0$, $\Delta t = 5.0 \times 10^{-6}$ s.

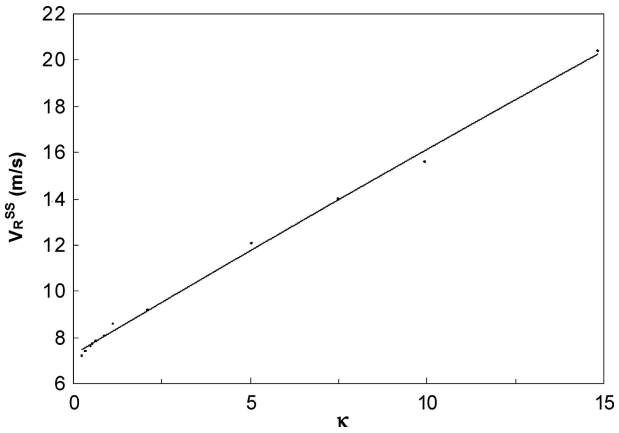

Figure 8 Steady-state reaction velocity, v_R^{ss}, versus κ for combustion synthesis of Mg_2Ni.

remains well above the temperature propagation velocity, v_T, defined here as:

$$v_T(t^*) = 2C(\kappa, T_0, T_a)\left(\frac{\alpha}{t^*}\right)^{1/2} \tag{21}$$

where the constant C is defined by means of the inverse error function, erf^{-1}, as:

$$C(\kappa, T_0, T_a) = \text{erf}^{-1}\left(\frac{T_{\text{eq}} - T_a}{T_0 - T_a}\right) \tag{22}$$

Equation (21) represents the integrated average of the instantaneous thermal front velocity over the characteristic time, t^* (i.e. the average of the time rate of change of the position of T_{eq}). T_{eq} represents the equilibrium temperature at the interface between two materials exhibiting different thermophysical properties and initial temperatures. For the case of uniform density and specific heat but varying thermal conductivity ($\rho_A = \rho_B$, $c_{p,A} = c_{p,B}$, $k_A \neq k_B$), T_{eq} is defined as:

$$T_{\text{eq}} = \left(\frac{k_p^{1/2}T_a + k_r^{1/2}T_0}{k_p^{1/2} + k_r^{1/2}}\right) = \left(\frac{\kappa^{1/2}T_a + T_0}{\kappa^{1/2} + 1}\right) \tag{23}$$

Fig. 9 shows the temperature-to-reaction propagation velocity ratio, v_T/v_R, as a function of κ for both the NiTi and Mg_2Ni systems. By definition, large ratios suggest that a significant amount of heat is able to diffuse ahead of the reaction. Conversely, small ratios indicate that the reaction front advances significantly faster than the average thermal velocity. Thus, this ratio can be interpreted as a measure of the average reaction zone thickness, δ_R, with lower ratios corresponding to narrower reaction zones. Over the range of interest in this investigation, the propagation ratio for Mg_2Ni is significantly lower than that of NiTi; for $\kappa \leq 0.5$, the difference exceeds one order-of-magnitude. These lower ratios suggest that the actual reaction zone in Mg_2Ni synthesis closely resembles the

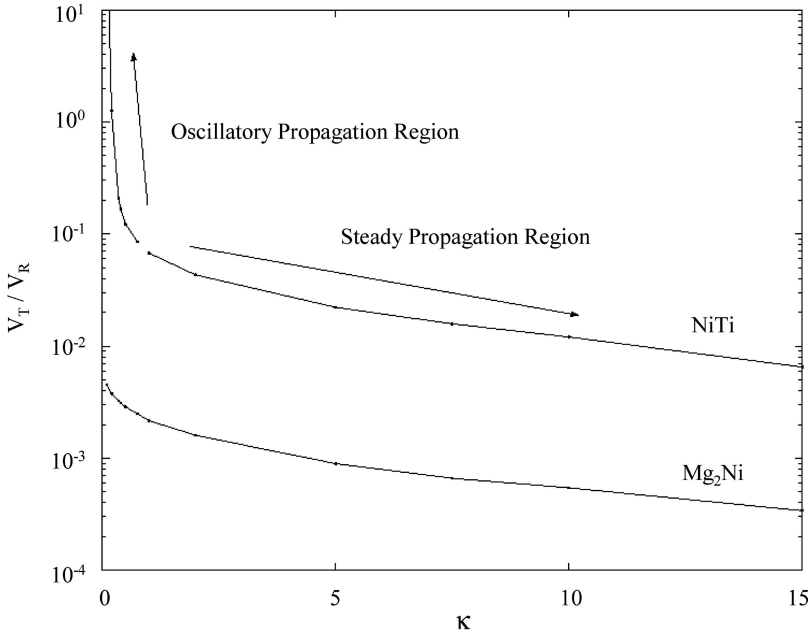

Figure 9 Temperature-reaction propagation velocity ratio as a function of κ.

ideal case ($\delta_R \to 0$); thus a steady propagation velocity approaching the maximum theoretical value is observed for all values of κ.

In the NiTi system however, a low κ has been shown to lead to oscillatory propagation. The relatively large propagation ratio in these cases indicates that the onset of oscillatory propagation is likely due to a degeneration of the reaction front. In other words, as v_T approaches v_R, enough heat diffuses into the unreacted material so as to initiate premature ignition well ahead of the reaction front rather than in just the immediately adjacent layer. This premature bulk reaction is then followed by a cooling period after which a normal reaction front develops once again. As the reaction intensifies, excessive heat is again allowed to diffuse ahead of the reaction zone. This process is self-repeating, producing temperature and concentration profiles such as those in Fig. 6. Fig. 10 shows a schematic representation of this process. Each cycle of oscillatory propagation begins with a coherent reaction front exhibiting a steep temperature gradient with only limited penetration into the unreacted material (Fig. 10(a)). As the reaction front proceeds with velocity, v_R, thermal diffusion raises the temperature of the reactants increasingly ahead of the reaction front. The rate of thermal diffusion into the unreacted material is represented here in terms of the average velocity, v_T, of the reactant-product interface equilibrium temperature, T_{eq} (Fig. 10(b)). Eventually, the higher temperature ahead of the reaction front leads to a significant increase in the reaction front velocity. This continues as the reaction front accelerates through the region affected by the thermal diffusion (Fig. 10(c)). A coherent reaction front again develops and the process repeats (Fig. 10(d)).

Further reductions in κ corresponding to even larger propagation ratios initially produce a decaying oscillatory

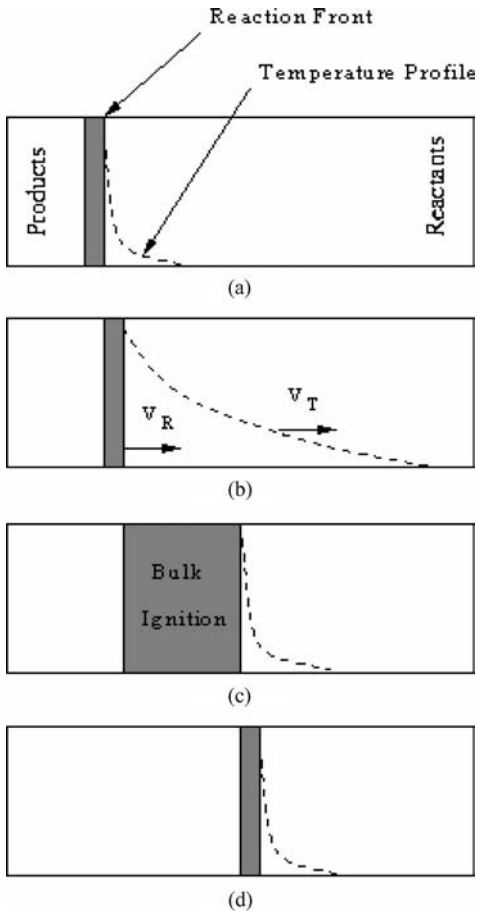

Figure 10 Schematic representation of oscillatory propagation during combustion synthesis: (a) each cycle begins with a coherent reaction front; (b) the high thermal diffusion rate causes the thermal velocity, v_T, to exceed the reaction velocity, v_R; (c) bulk ignition occurs in the preheated region; (d) a coherent front develops again and the process repeats.

front and subsequently, no observable reaction beyond the ignition surface. In these cases, dissipation of heat from the reaction front is too great to sustain the reaction to completion. Thus, the only reaction mode available for complete combustion appears to be bulk ignition throughout the entire compact by raising its internal temperature above the ignition point.

5. Conclusions

The effect of thermal conductivity on the combustion synthesis of intermetallics has been investigated. Specifically, a difference in the effective thermal conductivity on either side of the reaction front was studied to determine its influence on propagation behavior. A numerical model was developed to simulate the process, taking into account variations in k_{eff} as the reaction progresses. The governing equations were solved using a high-order-implicit numerical scheme capable of accommodating the steep spatial and temporal gradients of properties. The predicted results appear plausible and consistent with the trends presented in the available literature. However, a direct comparison with the experimental data was impossible due to the lack of detailed information on the change of effective thermal conductivity as the reaction progresses. The major findings of the study may be summarized thus:

- Increasing the ratio of the product conductivity to the reactant conductivity (κ) results in a higher propagation velocity.
- For moderately exothermic reactions, decreasing κ below a critical value leads to the onset of propagation instabilities (i.e. oscillatory propagation, bulk ignition).
- A larger κ corresponds to a thinner reaction zone.
- A larger κ leads to a higher steady-state combustion temperature.

The results obtained in this study can provide guidance in specifying stable and acceptable processing paths for the combustion synthesis of intermetallics. While the effective thermal conductivity of the unreacted phase has long been known to affect the behavior of the reaction front, it has been shown here that the ratio between the thermal conductivities of the reacted and unreacted material plays an equally significant role. Thus, it should be feasible to promote steady propagation or otherwise enhance the combustion behavior by adjusting the conductivity ratio, κ. This is easily accomplished through control of the initial compact porosity, reactant dilution, etc.

References

1. H. C. YI and J. J. MOORE, *J. Miner. Met. Mater. Soc.* **42** (8) (1990) 31.
2. Y. LU and M. HIROHASHI, *J. Mater. Sci. Lett.* **18** (5) (1999) 395.
3. B. Y. LI, L. J. RONG, Y. Y. LI and V. E. GJUNTER, *J. Mater. Res.* **15** (1) (2000) 10.
4. S. B. MARGOLIS, *Metallurg. Trans.* **23A** (1) (1992) 15.
5. Y. ZHANG and G. C. STANGLE, *J. Mater. Res.* **9** (10) (1994) 2592.
6. J. PUSZYNSKI, V. K. JAYARAMAN and V. HLAVACEK, *Int. J. Heat Mass Transf.* **28** (6) (1985) 1237.
7. L. RAO, P. YU and R. B. KANER, *J. Mater. Synth. Proc.* **2** (6) (1994) 343.
8. H. C. YI and J. J. MOORE, *J. Mater. Sci.* **24** (10) (1989) 3449.
9. *Idem.* 3456.
10. A. H. ADVANI, N. N. THADHANI, H. A. GREBE, R. HEAPS, C. COFFIN and T. KOTTKE, *J. Mater. Sci.* **27** (1992) 3309.
11. A. K. BHATTACHARYA, *J. Mater. Sci.* **27** (6) (1992) 1521.
12. *Idem. J. Am. Ceramic Soc.* **74** (9) (1991) 2113.
13. M. G. LAKSHMIKANTHA, A. BHATTACHARYA and J. A. SEKHAR, *Metallurg. Trans.* **23A** (1) (1992) 23.
14. J. PUSZYNSKI, J. DEGREVE and V. HLAVACEK, *Ind. Eng. Chem. Res.* **26** (7) (1987) 1424.
15. D. M. MATSON and Z. A. MUNIR, *Mater. Sci. Eng.* **153A** (1/2) (1992) 700.
16. Y. ZHANG and G. C. STANGLE, *J. Mater. Res.* **9** (10) (1994) 2605.
17. T. AKIYAMA, H. ISOGAI and J. I. YAGI, *AIChE J.* **44** (3) (1998) 695.
18. K. S. VECCHIO, J. C. LASALVIA, M. A. MEYERS and G. T. GRAY III, *Metallurg. Trans.* **23A** (1) (1992) 87.
19. S. K. LELE, *J. Comput. Phys.* **103** (1) (1992) 16.
20. M. CIMENT, S. H. LEVENTHAL and B. C. WEINBERG, *J. Comput. Phys.* **28** (2) (1978) 135.
21. R. S. HIRSH, *J. Comput. Phys.* **19** (1) (1975) 90.
22. Z. A. MUNIR, *Metallurg. Trans.* **23A** (1) (1992) 7.

Received 17 May
and accepted 29 August 2005